nature communications

Article

https://doi.org/10.1038/s41467-023-35984-5

Benchmark single-step ethylene purification from ternary mixtures by a customized fluorinated anion-embedded MOF

Received: 28 October 2022

Accepted: 11 January 2023

Published online: 25 January 2023

Check for updates

Yunjia Jiang,[1,4], Yongqi Hu,[1,4], Binquan Luan,[2], Lingyao Wang,[1], Rajamani Krishna,[3], Haofei Ni,[1], Xin Hu[1] & Yuanbin Zhang[1]

Ethylene (C_2H_4) purification from multi-component mixtures by physical adsorption is a great challenge in the chemical industry. Herein, we report a GeF_6^{2-} anion embedded MOF (ZNU-6) with customized pore structure and pore chemistry for benchmark one-step C_2H_4 recovery from C_2H_2 and CO_2. ZNU-6 exhibits significantly high C_2H_2 (1.53 mmol/g) and CO_2 (1.46 mmol/g) capacity at 0.01 bar. Record high C_2H_4 productivity is achieved from C_2H_2/CO_2/C_2H_4 mixtures in a single adsorption process under various conditions. The separation performance is retained over multiple cycles and under humid conditions. The potential gas binding sites are investigated by density functional theory (DFT) calculations, which suggest that C_2H_2 and CO_2 are preferably adsorbed in the interlaced narrow channel with high aff0inity. In-situ single crystal structures with the dose of C_2H_2, CO_2 or C_2H_4 further reveal the realistic host-guest interactions. Notably, rare C_2H_2 clusters are formed in the narrow channel while two distinct CO_2 adsorption locations are observed in the narrow channel and the large cavity with a ratio of 1:2, which accurately account for the distinct adsorption heat curves.

Ethylene (C_2H_4) is the foremost olefin as well as the highest volume product in the petrochemical industry, with an annual production capacity exceeding 214 million tons in 2021[1]. The manufacture of C_2H_4 and C_3H_6 accounts for 0.3% of global energy[2]. Current C_2H_4 production mainly relies on stream cracking of hydrocarbons[3–6]. Alternatively, oxidative coupling of methane (CH_4) has emerged as a promising technique to produce C_2H_4, among which acetylene (C_2H_2) and carbon dioxide (CO_2) are generated as byproducts and need to be deeply removed to produce polymer grade (>99.996%) C_2H_4[7]. Presently, multi-step purification process is adopted for purification of C_2H_4 from C_2H_4/C_2H_2/CO_2 mixtures in industry[8]. C_2H_2 is removed by catalytic hydrogenation using expensive noble-metal catalysts or solvent extraction, which is either energy intensive or associated with pollution[9,10]. CO_2 is removed by chemical adsorption using caustic soda, which causes huge waste of costly solvents[11].

Physical adsorption offers potential to significantly reduce the energy footprint of separation processes[12–21]. Nonetheless, C_2H_4 purification from ternary C_2H_4/C_2H_2/CO_2 mixtures remains an unmet challenge due to the similarity in molecular size and polarity (Supplementary Table 2), although separation of C_2H_2/C_2H_4[22–26] or C_2H_2/CO_2[27–32] binary mixtures has been realized by a plethora of porous materials. Besides, single-step purification of C_2H_4 from ternary C_2H_2/C_2H_4/C_2H_6[33,34] or quaternary C_2H_2/C_2H_4/C_2H_6/CO_2[35] mixtures has also been realized by several porous materials. To date, less than ten materials have been demonstrated to separate C_2H_4 from C_2H_4/C_2H_2/CO_2, including activated carbons, zeolites, covalent organic frameworks

[1]Key Laboratory of the Ministry of Education for Advanced Catalysis Materials, College of Chemistry and Life Sciences, Zhejiang Normal University, Jinhua 321004, China. [2]IBM Thomas J. Watson Research, Yorktown Heights, New York, NY 10598, USA. [3]Van't Hoff Institute for Molecular Sciences, University of Amsterdam, Science Park 904, 1098 XH Amsterdam, the Netherlands. [4]These authors contributed equally: Yunjia Jiang, Yongqi Hu.
e-mail: ybzhang@zjnu.edu.cn

and metal organic framework (MOFs)[36–39]. TIFSIX-17-Ni[36], NTU-65[37], and NTU-67[38] are so far the three optimal materials. TIFSIX-17-Ni[36] exhibits high C_2H_2/C_2H_4 and CO_2/C_2H_4 selectivity due to the negligible uptake of C_2H_4 under ambient condition. However, the capacity of C_2H_2 (3.30 mmol/g) and CO_2 (2.20 mmol/g) is relatively low due to the over-contracted channel. NTU-65[37] can selectively capture C_2H_2 and CO_2 by tuning the gate opening. However, the applied temperature must be at 263 K because lower temperatures lead to the adsorption of all the gases while higher temperatures cause the exclusion of CO_2. NTU-67[38] displays similar C_2H_2 (3.29 mmol/g) and CO_2 (2.04 mmol/g) capacity, but the C_2H_2/C_2H_4 and CO_2/C_2H_4 selectivity is greatly reduced as the C_2H_4 capacity (1.41 mmol/g) is relatively high. Additionally, the separation performance is deteriorated under humid conditions. Therefore, there is still a lack of ideal and stable materials to realize the simultaneous removal of C_2H_2 and CO_2 in $C_2H_2/CO_2/C_2H_4$ mixtures.

In this work, we reported a GeF_6^{2-} anion embedded MOF ZNU-6 (ZNU = Zhejiang Normal University) with large cages (~8.5 Å diameter) connected by narrow interlaced channels (~4 Å diameter) for benchmark one-step C_2H_4 recovery from C_2H_2 and CO_2. ZNU-6 is constructed by $CuGeF_6$ and tri(pyridin-4-yl)amine (TPA) and exhibits excellent chemical stability. Static gas adsorption isotherms showed that ZNU-6 takes up 1.53/8.06 mmol/g of C_2H_2 and 1.46/4.76 mmol/g of CO_2 at 0.01 and 1.0 bar (298 K), respectively. The calculated IAST selectivities for C_2H_2/C_2H_4 (1/99) and CO_2/C_2H_4 (1/99) are 43.8–14.3 and 52.6–7.8 (0.0001–1.0 bar), respectively. The calculated Q_{st} values at near-zero loading for C_2H_2 and CO_2 are 37.2 and 37.1 kJ/mol, indicative of its facility for material regeneration but much higher than that of C_2H_4 (29.0 kJ/mol). Modeling study indicates that there are two potential binding sites for C_2H_2, C_2H_4, and CO_2. One is in the interlaced channel and the other locates in the large cage. Moreover, all gas molecules prefer to be adsorbed in the interlaced channel with higher affinity. The realistic binding sites and host–guest interactions under normal conditions (298 K and 1.0 bar) were further demonstrated by in-situ single crystal structures with the saturated dose of gases. Notably, rare C_2H_2 clusters formed by π···π packing and C-H···C≡C interactions are observed in the interlaced channel with a small proportion of C_2H_2 molecules adsorbed in the large cage additionally. In sharp contrast, only 1/3 of CO_2 molecules are located in the narrow channel while 2/3 of CO_2 molecules are accommodated in the large cavity. This distinct gas distribution is highly consistent with the difference of adsorption heat curves. The practical C_2H_4 purification performance is further demonstrated by dynamic breakthroughs and record high C_2H_4 productivity is achieved from ternary $C_2H_2/CO_2/C_2H_4$ mixtures in a single adsorption process under various conditions. The separation performance is retained over multiple cycles and under humid conditions.

Results

Violet single crystals of ZNU-6 (Supplementary Fig. 1) were produced by layering a MeOH solution of TPA onto an aqueous solution of $CuGeF_6$ (Fig. 1a). X-ray crystal analysis revealed that ZNU-6 [$Cu_6(GeF_6)_6(TPA)_8$] crystallizes in a three-dimensional (3D) framework in the cubic Pm-3n space group. Every unit cell consists of six Cu^{2+} ions, six GeF_6^{2-} anions, and eight tridentate TPA ligands (Supplementary Table 1). The combination of Cu^{2+} and TPA produces a cationic pto network first (Fig. 1b), which determines the main pore size. The network is further embedded by GeF_6^{2-} pillar to give a ith-d topology framework with optimal pore chemistry (Fig. 1c). The frameworks are composed of large icosahedral cage-like pores (~8.5 Å) and interlaced narrow channels (~4 Å) (Fig. 1d–f). Each large cage is surrounded by 12 channels and every interlaced channel connects 4 cages. The adjacent two cages and two channels share the same GeF_6^{2-} anions at the edge. Both large pores and interlaced channels are abundant of Lewis basic F functional sites on the surface for gas binding. Such interconnected large cages and narrow channels are distinct from previous straight 1D channels of anion pillared MOFs (e.g., SIFSIX-1-Cu, SIFSIX-3-Ni). Besides, the narrow channel size may provide kinetic selectivity for C_2H_2 (3.3 Å) and CO_2 (3.3 Å) given their small molecular size compared to C_2H_4 (4.2 Å). Thus, ZNU-6 with abundant functional GeF_6^{2-} binding sites, high porosity for C_2H_2 and CO_2 accommodation and narrow channel for kinetic preference features the promising characteristics for efficient purification of C_2H_4 from ternary $C_2H_2/CO_2/C_2H_4$ mixture.

The intrinsic porosity of ZNU-6 was investigated by N_2 adsorption at 77 K. As shown in Fig. 2a, ZNU-6 exhibited a type I adsorption isotherm. The Brunauer–Emmett–Teller surface area and pore volume were calculated to be 1330.3 m^2/g and 0.554 cm^3/g (Supplementary Fig. 10). The calculated pore size ranges from 8.22 to 10.76 Å with the summit in 9.0 Å, highly close to the pore aperture of ~8.5 Å evaluated from the single crystal structure (Fig. 2a). Then, single-component adsorption isotherms of C_2H_2, CO_2, and C_2H_4 were collected at 298 K (Fig. 2b). At 1.0 bar, the C_2H_2 and CO_2 uptakes are 8.06 and 4.76 mmol/g, higher than those of most APMOFs (Fig. 2c). The capacities are equal to 4.68 and 2.77 gas molecules per GeF_6^{2-} anion. Such high C_2H_2/anion and CO_2/anion uptakes have never been realized in anion pillared MOFs (Supplementary Table S7)[36–38,40–44]. Particularly, C_2H_2/anion and CO_2/anion uptakes in benchmark TIFSIX-17-Ni[36], SIFSIX-17-Ni[36] and NTU-67[38] are only 1.36/0.91, 1.29/0.9 and 2.06/1.28, respectively (Supplementary Fig. 25). So far, isomorphic SIFSIX-Cu-TPA[40] displays the ever highest C_2H_2/anion (4.44) uptake while SIFSIX-1-Cu[41] displays the ever highest CO_2/anion (2.72) uptake. It is worth mentioning that these records have been marginally surpassed by ZNU-6's (Supplementary Fig. 25). Notably, the uptakes of C_2H_2 and CO_2 on ZNU-6 at 0.01 bar are as high as 1.53 and 1.46 mmol/g, superior to those of all the porous materials in the context of ternary $C_2H_2/CO_2/C_2H_4$ separation, such as TIFSIX-17-Ni (1.38/0.32 mmol/g)[36], SIFSIX-17-Ni (0.91/0.20 mmol/g)[36], NTU-67 (0.47/0.65 mmol/g)[38], and TpPa-NO_2 (0.17/0.03 mmol/g)[39]. At 0.1 bar, the capacities of C_2H_2 and CO_2 reach up to 4.64 and 2.21 mmol/g (Fig. 2b), even higher than the uptakes of many porous materials at 1 bar and 298 K, for example, TIFSIX-17-Ni (3.30/2.20 mmol/g)[36]. In the meantime, the C_2H_4 uptakes on ZNU-6 at 0.01 and 0.1 bar are only 0.15 and 1.07 mmol/g, much lower than those of C_2H_2 and CO_2 under the same conditions. The C_2H_2, CO_2, and C_2H_4 adsorption isotherms were further collected at 278 and 308 K (Fig. 2d). The adsorption capacities of C_2H_2 and CO_2 at 1 bar increase to 8.74 and 6.26 mmol/g at 278 K. As selectivity is also an important parameter to assess the separation performance, we further calculated the C_2H_2/C_2H_4 and CO_2/C_2H_4 selectivities on ZNU-6 using ideal adsorbed solution theory (IAST) after fitting isotherms into dual site Langmuir or single site Langmuir equation with excellent accuracy. The IAST selectivity for 1/99 C_2H_2/C_2H_4 is 43.8–14.3 (Fig. 2e), higher than those of NTU-67 (8.1)[38] and TpPa-NO_2 (5.9)[39]. The IAST selectivities for 1/99 CO_2/C_2H_4 mixture is also as high as 52.6-7.8 (Fig. 2e). Besides, both C_2H_2/C_2H_4 and CO_2/C_2H_4 selectivity on ZNU-6 is improved with the pressure decrease or the increase of C_2H_4 ratios (from 90% to 99%) in the binary mixtures (Supplementary Figs. 13, 14), indicating ZNU-6 is favored for trace C_2H_2 and CO_2 capture from bulky C_2H_4 mixtures. Apart from the IAST selectivity, the Henry coefficients were also calculated to evaluate the Henry's selectivity of ZNU-6 (Supplementary Figs. 15–17), the Henry's selectivity for C_2H_2/C_2H_4 and CO_2/C_2H_4 is 8.2 and 7.8, respectively, superior to those of NTU-67 (2.4/4.2)[38] and TpPa-NO_2 (4.0/1.8)[39] (Supplementary Tables 4, 5). We further calculated the isosteric enthalpy of adsorption (Q_{st}) for ZNU-6 by using the Clausius-Clapeyron equation. Q_{st} values at near-zero loading for C_2H_2, CO_2, and C_2H_4 are 37.2, 37.1, and 29.0 kJ/mol (Fig. 2f), respectively, indicative of the preferred affinity of C_2H_2 and CO_2 over C_2H_4. Notably, the Q_{st} values for C_2H_2 and CO_2 on ZNU-6 are only modestly high and slightly lower than those of many top-performing materials in the context of C_2H_4 purification, such as SIFSIX-17-Ni (44.2/40.2 kJ/mol)[36], TIFSIX-17-Ni (48.3/37.8 kJ/mol)[36], and NTU-67 (44.1/41.5 kJ/mol)[38]. Such moderate Q_{st} endows facile regeneration of ZNU-6 under mild conditions.

https://doi.org/10.1038/s41467-023-35984-5

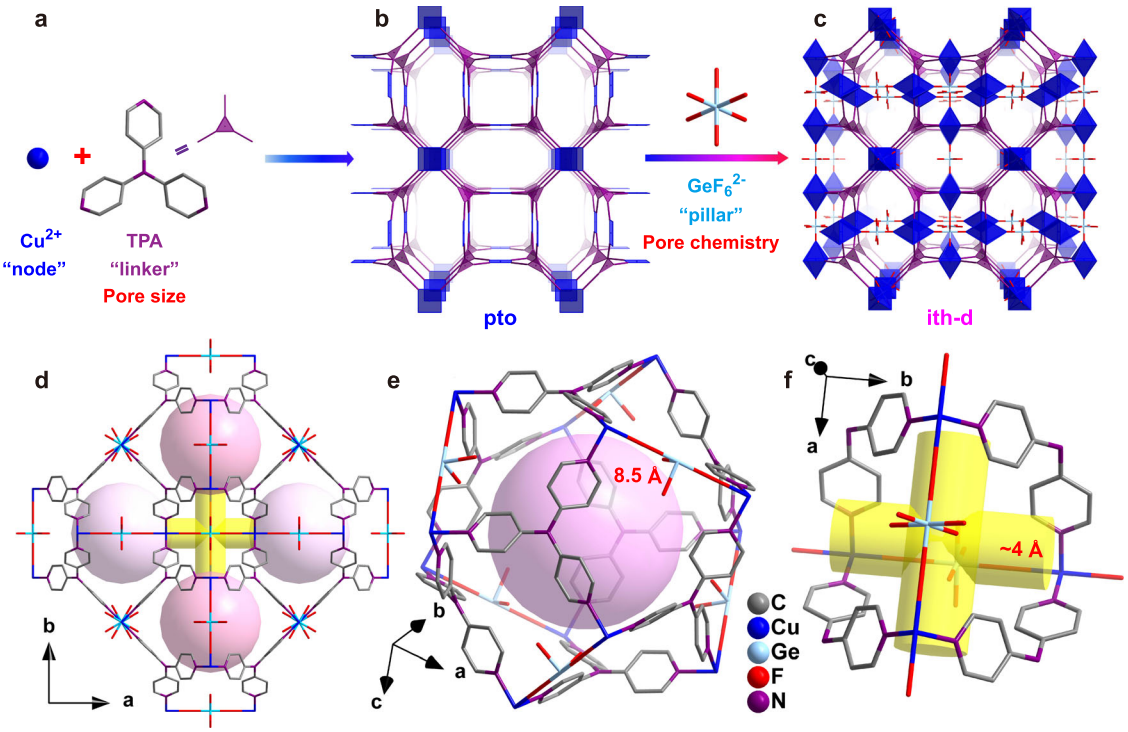

Fig. 1 | Porous structure of ZNU-6. a–c Exquisite control of pore size/shape and pore chemistry in ZNU-6 from pillared (3,4)-connected pto network to GeF_6^{2-} embedded ith-d topology framework; **d** Overview of ZNU-6 structure with cage-like pores and interlaced channels. **e** Structure and size of the cage-like pore. **f** Structure and size of the interlaced channel connecting four cages.

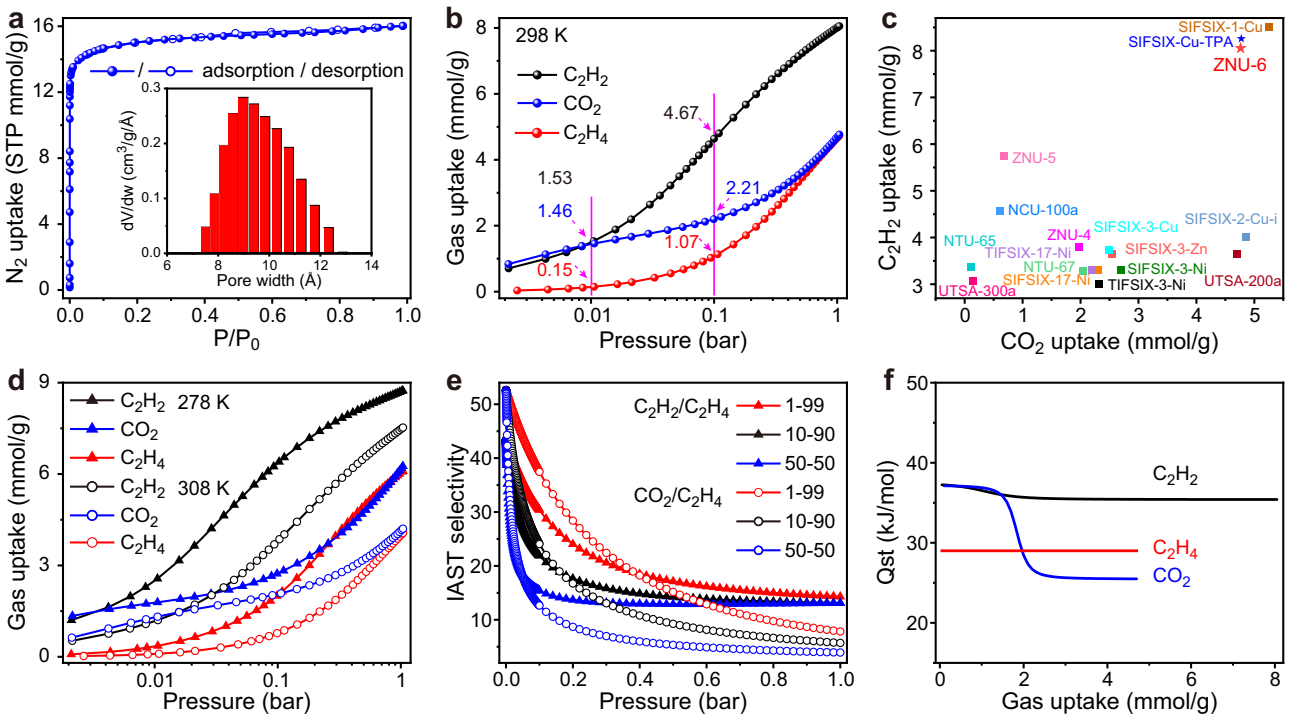

Fig. 2 | The sorption performance. a N_2 adsorption and desorption isotherms for ZNU-6 and the calculated pore size distribution. **b** C_2H_2, CO_2, and C_2H_4 adsorption isotherms of ZNU-6 at 298 K. **c** Comparison of the saturated C_2H_2 and CO_2 uptake (1 bar, 298 K) among anion pillared MOFs. **d** C_2H_2, CO_2, and C_2H_4 adsorption isotherms of ZNU-6 at 278/308 K. **e** C_2H_2/C_2H_4 and CO_2/C_2H_4 IAST selectivity of ZNU-6 at 298 K. **f** Q_{st} of C_2H_2, CO_2, and C_2H_4 in ZNU-6. Source data are provided as a Source Data file.

https://doi.org/10.1038/s41467-023-35984-5

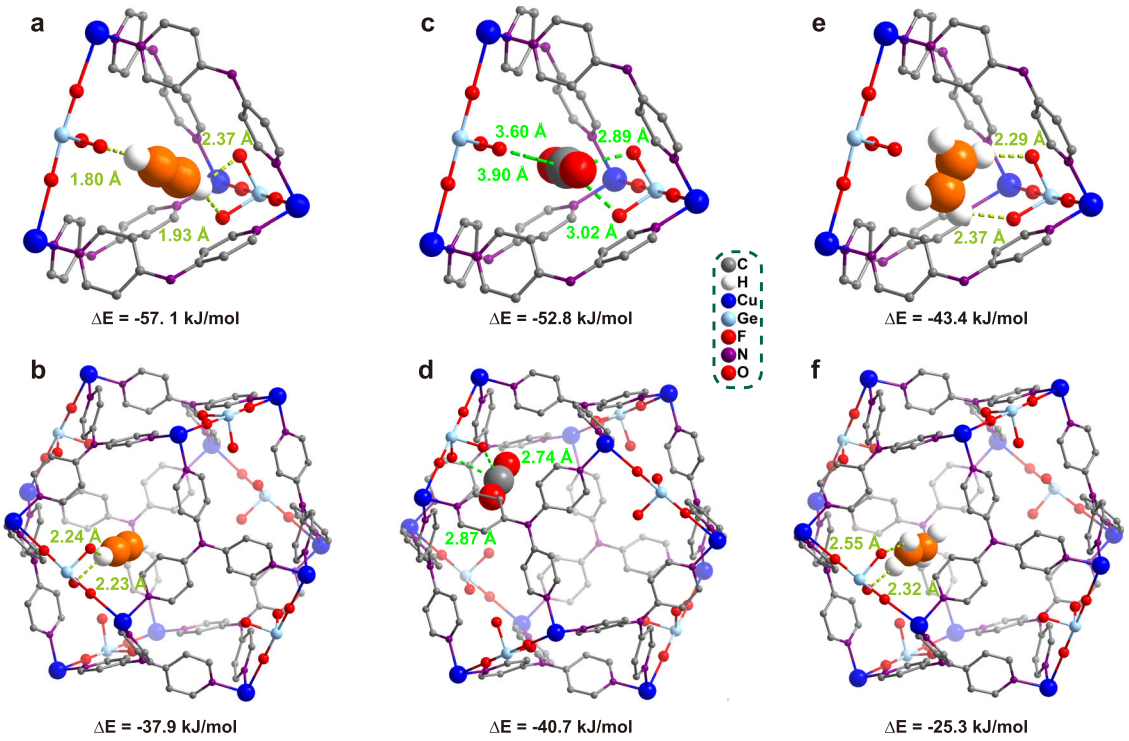

Fig. 3 | The DFT optimized gas adsorption configuration. Binding sites I, II of C_2H_2 (**a, b**), CO_2 (**c, d**), and C_2H_4 (**e, f**).

To gain more insights into the gas adsorption behavior, density functional theory (DFT)-based calculations (see Method section) were applied to identify the adsorption configuration and binding energies of C_2H_2, CO_2, and C_2H_4. For all gases, two different binding sites were observed. Site I is in the interlaced channel and Site II is in the large cavity (Fig. 3). For C_2H_2 in Site I, the two hydrogen atoms interact strongly with three F atoms with the distances of 1.80, 1.93, and 2.37 Å. The calculated binding energy is 57.1 kJ/mol (Fig. 3a). As for C_2H_2 adsorbed in Site II, only one hydrogen atom can interact with the adjacent F atoms with the distance of 2.23 and 2.24 Å, and the corresponding binding energy decreases to 37.9 kJ/mol (Fig. 3b), indicating that C_2H_2 is preferentially adsorbed in the narrow channel. The same results are also observed for CO_2 and C_2H_4, the binding energies in the channel are much higher than those in the large cage. In Site I, CO_2 is trapped by two strong and two weak electrostatic F···C=O interactions in the distance of 2.89, 3.02, 3.60, and 3.90 Å, the binding energy is 52.8 kJ/mol (Fig. 3c); C_2H_4 is adsorbed via two F···H interactions (2.29 and 2.37 Å) with the binding energy of 43.3 kJ/mol (Fig. 3e). In Site II, the binding energy of CO_2 drops to 40.7 kJ/mol with the number of electrostatic F···C=O interactions (2.74 and 2.87 Å) decreasing to two (Fig. 3d); the binding energy of C_2H_4 reduces to 25.3 kJ/mol with the length of F···H extending to 2.55 and 2.32 Å (Fig. 3f). In addition, it is notable that either in Site I or II, the binding energy of C_2H_2 or CO_2 is superior to that of C_2H_4, confirming that the adsorption of C_2H_2 or CO_2 in ZNU-6 is more preferable than that of C_2H_4.

Although DFT calculations have identified two different binding sites for each gas, it is still difficult to understand the distinct adsorption heat curves. Therefore, we further studied the in-situ structures of ZNU-6 with gas loading (Fig. 4). We found that averagely 25.78 C_2H_2, 18 CO_2, or 13.07 C_2H_4 molecules can be adsorbed per unit cell of ZNU-6 (Supplementary Table 1), corresponding to 4.3 C_2H_2, 3.0 CO_2, and 2.2 C_2H_4 molecules for each GeF_6^{2-} anion, which are close to the saturated values from gas adsorption isotherms (4.63 C_2H_2, 2.77 CO_2, and 2.75 C_2H_4). Both of C_2H_2 and CO_2 have two binding sites, i.e., Site I in the interlaced channel and Site II in the large cage. Notably, the amount of C_2H_2 molecules distributed to the two locations is 3.8 and 0.5 per GeF_6^{2-} anion while that for CO_2 is 1 and 2 per GeF_6^{2-} anion (Fig. 4a, b). Such different gas distribution can precisely account for the C_2H_2 Q_{st} curve with a modest decrease and the CO_2 Q_{st} curve with a sharp decrease along the gas loading. Specifically, C_2H_2 molecules adsorbed in Site I bind to F atoms on the surface of the channels via multiple cooperative hydrogen bonds (C-H···F = 1.97–2.55 Å), and the others in Site II interact F atoms via single H···F hydrogen bond with the distance of 2.51 Å (Fig. 4a and Table 1). Besides, the C_2H_2 molecules in Site I aggregate to form a stacked gas cluster by π···π packing and C-H···C≡C interactions, which has rarely been observed previously. Regarding CO_2, it is trapped by F···C=O electrostatic interaction in Site I and II (Fig. 4b). The only difference is that the C···F distance is 2.64 Å in Site I and 2.80 Å in Site II (Table 1). From the single crystal structure, two different CO_2 molecules that are very close and opposite to each other in the narrow channel (site I) are observed. However, these two CO_2 molecules cannot exist in the same narrow channel at the same time and thus both CO_2 molecules display the occupancy of 50%. In Site II, the C atom of CO_2 is ordered while the O atoms are disordered to two perpendicular positions with the occupancy of 50% for each configuration. Besides, the linear CO_2 molecules are slightly bent due to the strong attraction from GeF_6^{2-} anion. The bent angle of 157.5° (in Site I) and 170.8° (in Site II) are consistent with the interaction strength. In term of C_2H_4, only one site in the narrow channel is found. The C atoms of C_2H_4 molecule are ordered while the H atoms are disordered. The distances of C-H···F interactions between C_2H_4 and framework are 2.31–2.64 Å (Fig. 4c and Table 1). Considering the slight lower C_2H_4/GeF_6^{2-} ratio observed in the single crystal structure, there should be some C_2H_4 molecules adsorbed in the large cage. However, due to the probable disorder of C_2H_4 molecules over the whole cage, the C_2H_4 molecules in Site II were not solved. Nonetheless, this uniform adsorption configuration is consistent with the flat Q_{st} curve for C_2H_4.

Apart from the C_2H_2, CO_2, or C_2H_4 molecules, some water molecules were also identified in the framework (Supplementary Fig. 4). As there is still a lot of space in the large cavity after saturated adsorption of C_2H_2, CO_2, or C_2H_4 gases at 100 kPa, the water adsorption behavior probably occurred during the single crystal measurement, which is

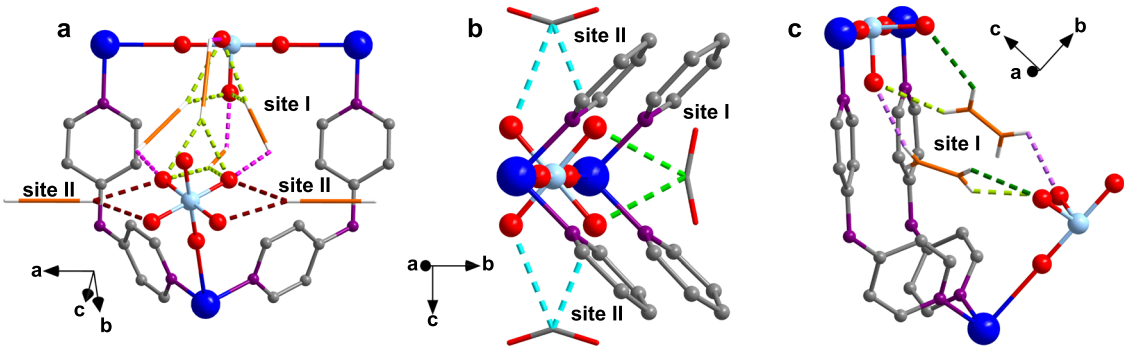

Fig. 4 | Single crystal structure of gas-loaded ZNU-6. a C_2H_2 @ ZNU-6 [$Cu_6(GeF_6)_6(TPA)_8$ $(C_2H_2)_{25.78}$]; **b** CO_2 @ ZNU-6 [$Cu_6(GeF_6)_6(TPA)_8$ $(CO_2)_{18}$]; **c** C_2H_4 @ ZNU-6 [$Cu_6(GeF_6)_6(TPA)_8$ $(C_2H_4)_{13.07}$].

exposed to air. Interestingly, these water molecules are distant from GeF_6^{2-}, indicating that these H_2O molecules do not occupy the binding sites for the targeted gases. Instead, some unique interactions are observed between the gas molecules and water molecules, e.g., O-H···C=O hydrogen bonds between CO_2 and H_2O. Notably, our resolved single crystal structures show completely different C_2H_2 and CO_2 adsorption configurations from those of isomorphic SIFSIX-Cu-TPA for C_2H_2/CO_2 separation in Wu's work[39].

Motivated by the high adsorption capacity and selectivity in single-component adsorption as well as the in-situ single crystal structure analysis, breakthrough experiments were conducted for C_2H_2/C_2H_4, CO_2/C_2H_4, and $C_2H_2/CO_2/C_2H_4$ mixtures. The results showed that highly efficient separations can be accomplished by ZNU-6 for all the gas mixtures under various conditions. For 1/99 C_2H_2/C_2H_4 mixtures, C_2H_4 is eluted at 12 mins while C_2H_2 is detected until 192 min. For 10/90 CO_2/C_2H_4 mixtures, C_2H_4 and CO_2 are detected at 12 and 43.5 min, respectively (Fig. 5a). For 1/1/98 $C_2H_2/CO_2/C_2H_4$ mixtures, C_2H_2 and CO_2 broke out simultaneously and 64.42 mol/kg of polymer grade C_2H_4 is produced by single adsorption process (Fig. 5b). The productivity is improved to 80.89 mol/kg when decreasing the temperature to 283 K (Supplementary Fig. 46). The CO_2 breakthrough time becomes shortened with the increase of CO_2 ratio, which is 72 and 52 min for 1/5/94 (Figs. 5c) and 1/9/90 (Fig. 5d) $C_2H_2/CO_2/C_2H_4$ mixtures. The polymer grade C_2H_4 productivity is 21.37 and 13.81 mol/kg, respectively. As most reported C_2H_4 productivity from $C_2H_2/CO_2/C_2H_4$ mixtures are compared under 1/9/90, a comparison plot of the C_2H_4 productivity and dynamic C_2H_2 capacity from 1/9/90 $C_2H_2/CO_2/C_2H_4$ mixtures is presented in Fig. 5e. ZNU-6 displays the record high C_2H_4 productivity and second highest C_2H_2 dynamic capacity. The C_2H_4 productivity of ZNU-6 is >2.5 folds of the previous benchmark of NTU-67 (5.42 mol/kg)[38]. C_2H_4 productivity with the unit of mol/kg/h is also calculated for comparison (Supplementary Table S10). ZNU-6 with the productivity of 15.93 mol/kg/h is the highest reported value.

In view of the importance of the recyclability and stability of porous materials for practical applications, the water and thermal stability of ZNU-6 was investigated. There was no noticeable loss in the CO_2 adsorption capacity after six cycles of adsorption/desorption experiments (Supplementary Fig. 26). Long time soaking of ZNU-6 in water or polar organic solvents such as DMSO, DMF and MeCN did not change the porous structure of ZNU-6, as demonstrated by the PXRD patterns as well as the gas adsorption isotherms (Supplementary Fig. 7). Thermogravimetric analysis (TGA) and temperature varied PXRD indicated ZNU-6 is stable below 200 °C (Supplementary Figs. 8, 9). Breakthroughs under humid conditions or over four cycles preserved nearly the identical separation performance (Fig. 5f). Although many water molecules can be adsorbed in ZNU-6, as described in in-situ crystals and water adsorption isotherms (Supplementary Fig. 27), the presence of humid has negligible influence on the separation performance (Fig. 5f). This is probably due to the co-adsorption of water and target gases as well as the fast $C_2H_2/CO_2/C_2H_4$ diffusion kinetics (Supplementary Fig. 29–31).

Table 1 | The distances of the host–guest interactions

Crystals	Site I	Site II
25.78 C_2H_2 @ ZNU-6	1.97/2.55 Å (C-H···F)	2.51 Å (C-H···F)
18 CO_2 @ ZNU-6	2.64 Å (C···F)	2.80 Å (C···F)
13.07 C_2H_4 @ ZNU-6	2.31/2.54/2.64 Å (C-H···F)	-

Discussion

In conclusion, we reported a GeF_6^{2-} anion embedded metal organic framework ZNU-6 with optimal pore structure and pore chemistry for benchmark one-step C_2H_4 purification by simultaneous removal of C_2H_2 and CO_2. ZNU-6 exhibits remarkably high C_2H_2 and CO_2 capacity under both low and high pressures. The C_2H_2/anion and CO_2/anion uptakes are the highest among all the anion pillared MOFs. 64.42, 21.37, 13.81 mol/kg polymer grade C_2H_4 can be produced from $C_2H_2/CO_2/C_2H_4$ (1/1/98, 1/5/94, 1/9/90) mixtures, all superior to the previous benchmarks. The separation performance is sustained over multiple cycles or under humid conditions. The potential gas binding sites are investigated by DFT calculation, which indicate that C_2H_2 and CO_2 are preferentially adsorbed in the interlaced narrow channel with high affinity. In-situ single crystal structures with the dose of C_2H_2, CO_2 or C_2H_4 further reveal the realistic host–guest interactions, accounting for the distinct shapes of the adsorption heat curves. In general, our work highlights the significance of regulating pore structure and pore chemistry in porous materials to construct multiple cooperative functionalities for gas separation.

Methods

Synthesis of ZNU-6

To a 5 mL long thin tube was added a 1 mL of aqueous solution with $Cu(NO_3)_2{\cdot}3H_2O$ (~1.3 mg) and $(NH_4)_2GeF_6$ (~1.0 mg). 2 mL of MeOH/H_2O mixture (v:v = 1:1) was slowly layered above the solution, followed by a 1 mL of MeOH solution of TPA (~1.0 mg). The tube was sealed and left undisturbed at 298 K. After ~1 week, purple single crystals were obtained.

Preparation of gas loaded ZNU-6

The crystalline sample of ZNU-6 was filled into a glass tube and heated at 120 °C under vacuum for 24 h. After the sample cooling down, CO_2, C_2H_2, or C_2H_4 was introduced into the sample respectively with Builder SSA 7000 (Beijing) instrument until the pressure reach to 1 bar at 298 K and the state is maintained for another hour. Then, the crystals were picked out, covered with the degassed oil, and single crystal X-ray diffraction measurements were then carried out at 298 K as soon as possible.

https://doi.org/10.1038/s41467-023-35984-5

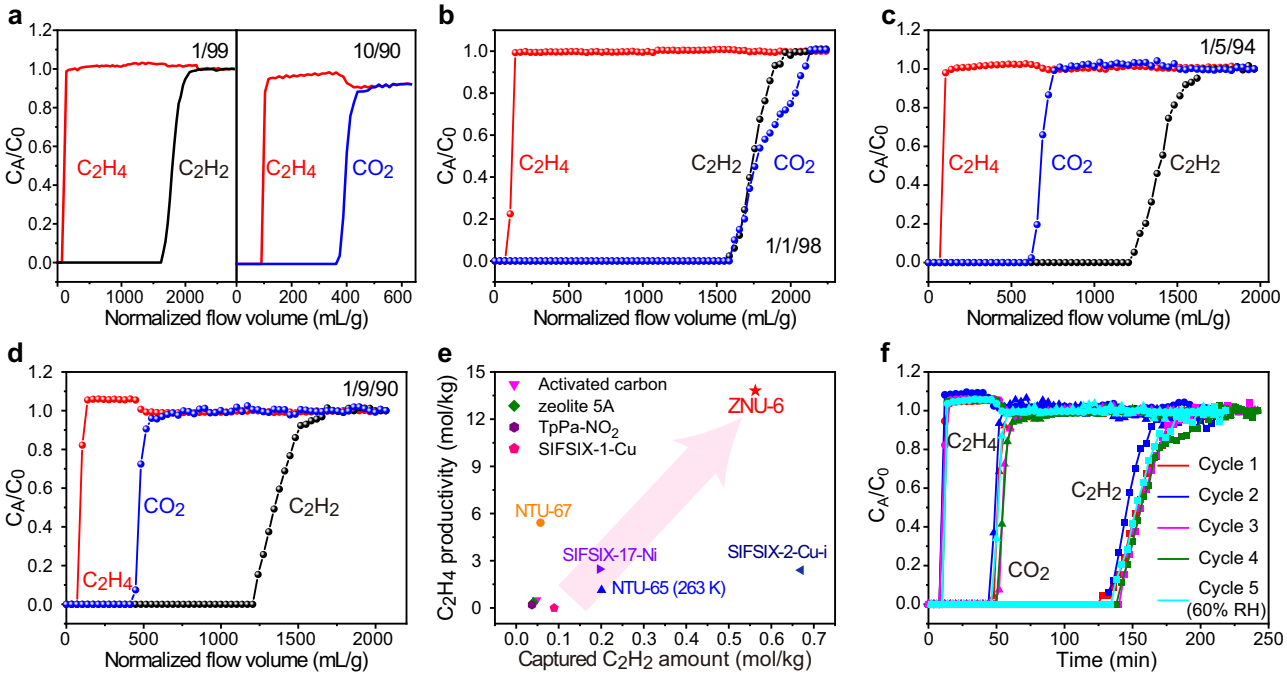

Fig. 5 | C_2H_4 purification. Experimental breakthrough curves of ZNU-6 for binary mixture **a** C_2H_2/C_2H_4 (1/99) and CO_2/C_2H_4 (10/90) at 298 K. Experimental breakthrough curves of ZNU-6 for ternary mixture **b** $C_2H_2/CO_2/C_2H_4$ (1/1/98), **c** $C_2H_2/CO_2/C_2H_4$ (1/5/94), and **d** $C_2H_2/CO_2/C_2H_4$ (1/9/90). **e** Comparison of the captured C_2H_2 amount and C_2H_4 productivity from $C_2H_2/CO_2/C_2H_4$ (1/9/90) ternary mixture. **f** Five cycles of experimental breakthrough curves of ZNU-6 for $C_2H_2/CO_2/C_2H_4$ (1/9/90) at 298 K (1–4: dry condition, 5: humid condition). Source data are provided as a Source Data file.

Single-crystal X-ray diffraction

Single-crystal X-ray diffraction studies were conducted on the BrukerAXS D8 VENTURE diffractometer equipped with a PHOTON-100/CMOS detector (GaKα, $\lambda = 1.34139$ Å). Indexing was performed using APEX2. Data integration and reduction were completed using SaintPlus 6.01. Absorption correction was performed by the multi-scan method implemented in SADABS. The space group was determined using XPREP implemented in APEX2.1 The structure was solved with SHELXS-97 (direct methods) and refined on F2 (nonlinear least-squares method) with SHELXL-97 contained in APEX2, WinGX v1.70.01, and OLEX2 v1.1.5 program packages. All non-hydrogen atoms were refined anisotropically. The contribution of disordered solvent molecules was treated as diffuse using the Squeeze routine implemented in Platon.

Powder X-ray diffraction

Powder X-ray diffraction (PXRD) data were collected on the SHIMADZU XRD-6000 diffractometer (Cu Kα$\lambda = 1.540598$ Å) with an operating power of 40 kV, 30 mA and a scan speed of 4.0°/min. The range of 2θ was from 5° to 50°.

Thermal gravimetric analysis

Thermal gravimetric analysis was performed on the TGA STA449F5 instrument. Experiments were carried out using a platinum pan under nitrogen atmosphere which conducted by a flow rate of 60 mL/min nitrogen gas. The data were collected at the temperature range of 50 °C to 600 °C with a ramp of 10 °C /min.

The static gas/vapor adsorption equilibrium measurements

The static gas adsorption equilibrium measurements were performed on the Builder SSA 7000 instrument. The water vapor adsorption equilibrium measurements were performed on the BeiShiDe DVS instrument. Before measurements, the sample of ZNU-6 (~100 mg) was evacuated at 25 °C for 2 h firstly, and then at 120 °C for 12 h until the pressure dropped below 7 μmHg. The sorption isotherms were collected at 77 K, 278, 298, and 308 K on activated samples. The experimental temperatures were controlled by liquid nitrogen bath (77 K) and water bath (278, 298, and 308 K), respectively.

Breakthrough experiments

The breakthrough experiments were carried out on a dynamic gas breakthrough equipment. The experiments were conducted using a stainless steel column (4.6 mm inner diameter × 50 mm length). The weight of ZNU-6 powder packed in the columns were 0.5806 g. The column was activated at 75 °C for 2 h under vacuum, and then raised to 120 °C for overnight. The mixed gas of C_2H_2/C_2H_4 (1/99, v/v), CO_2/C_2H_4 (10/90, v/v), or $C_2H_2/CO_2/C_2H_4$ (1/9/90, 1/5/94, 1/1/98, 5/5/90, v/v/v) was then introduced. $C_2H_2/CO_2/C_2H_4$ mixtures are produced by mixing three pure gases or mixing binary mixture with pure gas. Every flowrate was calibrated by self-made soap film flowmeter. Outlet gas from the column was monitored using gas chromatography (GC-9860-5CNJ) with the thermal conductivity detector TCD. After the breakthrough experiment, the sample was regenerated with an Ar flow of 5 mL min^{-1} under 120 °C for 8 h or under vacuum at 120 °C for 8 h.

Fitting of experimental data on pure component isotherms

The unary isotherms for C_2H_2 and CO_2 measured at three different temperatures 278 K, 298 K, and 308 K in ZNU-6 were fitted with excellent accuracy using the dual-site Langmuir model, where we distinguish two distinct adsorption sites A and B:

$$q = \frac{q_{sat,A} b_A p}{1 + b_A p} + \frac{q_{sat,B} b_B p}{1 + b_B p} \tag{1}$$

In Eq (S1), the Langmuir parameters b_A,b_B are both temperature dependent

$$b_A = b_{A0} \exp\left(\frac{E_A}{RT}\right); b_b = b_{B0} \exp\left(\frac{E_B}{RT}\right) \tag{2}$$

In Eq. (2), E_A,E_B are the energy parameters associated with sites A, and B, respectively.

The corresponding unary isotherms for C_2H_4 measured at three different temperatures 278 K, 298 K, and 308 K in ZNU-6 were fitted with excellent accuracy using the single-site Langmuir model.

$$q = \frac{q_{sat,A} b_A p}{1 + bp} \tag{3}$$

The unary isotherm fit parameters for C_2H_2, CO_2, and C_2H_4 are provided in Table S1.

IAST calculations

The adsorption selectivity for separation of binary mixtures of species 1 and 2 is defined by

$$S_{ads} = \frac{q_1/q_2}{p_1/p_2} \tag{4}$$

where q_1, q_2 are the molar loading (units: mol kg^{-1}) in the adsorbed phase in equilibrium with a gas mixture with partial pressures p_1, p_2 in the bulk gas.

Calculation of isosteric heat of adsorption (Q_{st})

The isosteric heat of adsorption, Q_{st}, is defined as

$$Q_{st} = -RT^2 \left(\frac{\partial \ln p}{\partial T}\right)_q \tag{5}$$

where the derivative in the right member of Eq. (5) is determined at constant adsorbate loading, q. The calculations are based on the Clausius-Clapeyron equation.

Density functional theory calculation

In this work, the DFT-based calculations were carried out using the CP2K package[45]. The Perdew-Burke-Ernzerhof (PBE) exchange functional[46], Gaussian plane wave (PAW) pseudopotentials[47] and DZVP basis sets[48] for carbon, oxygen, fluorine, nitrogen, germanium and copper atoms, were used to describe the exchange–correlation interactions and electron–ion interaction, respectively. At the same time, the PBE-D3 method[49] with Becke–Jonson damping for all atoms and Hubbard U corrections for the open-shell 3d transition metal (Cu) was used for geometry optimizations. The U value of 5.0 eV was used in this study. In all calculations, the net charges of simulation systems were set to zero. The adsorption energy can be obtained from formula below:

$$E_{ads} = E_{adsorbate+substrate} - E_{substrate} - E_{adsorbate} \tag{6}$$

where $E_{adsorbate+substrate}$ and $E_{substrate}$ were the total energies of the substrate with and without adsorbate, and $E_{adsorbate}$ was the energy of the adsorbate.

Data availability

The authors declare that the data supporting the findings of this study are available within the article and Supplementary Information. The X-ray crystallographic data related to ZNU-6 have been deposited at the Cambridge Crystallographic Data Centre (CCDC), under deposition numbers 2192744–2192747, respectively. These data can be obtained free of charge from the CCDC via www.ccdc.cam.ac.uk/data_request/cif. The data that support the findings of this study are available from the corresponding author. Besides, Source data are provided with this paper.

References

1. Fernández, L. Global production capacity of ethylene 2018–2021, https://www.statista.com/statistics/1067372/global-ethylene-production-capacity/ (2022).
2. Sholl, D. S. & Liverly, R. P. Seven chemical separations to change the world. *Nature* **532**, 435–437 (2016).
3. Wang, Q. et al. One-step removal of alkynes and propadiene from cracking gases using a multi-functional molecular separator. *Nat. Commun.* **13**, 2955 (2022).
4. Suo, X. et al. Synthesis of ionic ultramicroporous polymers for selective separation of acetylene from ethylene. *Adv. Mater.* **32**, 1907601 (2020).
5. Li, J. et al. Metal-organic framework containing planar metal-binding sites: efficiently and cost-effectively enhancing the kinetic separation of C_2H_2/C_2H_4. *J. Am. Chem. Soc.* **141**, 3807–3811 (2019).
6. Sahoo, R. et al. C_{2s}/C_1 hydrocarbon separation: the major step towards natural gas purification by metal-organic frameworks (MOFs). *Coord. Chem. Rev.* **442**, 213998 (2021).
7. Farrell, B. L. et al. A viewpoint on direct methane conversion to ethane and ethylene using oxidative coupling on solid catalysts. *ACS Catal.* **6**, 4340–4346 (2016).
8. Chen, K.-J. et al. Synergistic sorbent separation for one-step ethylene purification from a four-component mixture. *Science* **366**, 241–246 (2019).
9. Zhang, R. et al. The cost-effective Cu-based catalysts for the efficient removal of acetylene from ethylene: the effects of Cu valence state, surface structure and surface alloying on the selectivity and activity. *Chem. Eng. J.* **351**, 732–746 (2018).
10. Huang, Y. et al. Separation of light hydrocarbons with ionic liquids: a review. *Chin. J. Chem. Eng.* **27**, 1374–1382 (2019).
11. Ren, T. et al. Olefins from conventional and heavy feedstocks: energy use in steam cracking and alternative processes. *Energy* **31**, 425–451 (2006).
12. Chai, Y. et al. Control of zeolite pore interior for chemoselective alkyne/olefin separations. *Science* **368**, 1002–1006 (2020).
13. Li, H. et al. Porous metal-organic frameworks for gas storage and separation: status and challenges. *EnergyChem* **1**, 100006 (2019).
14. Adil, K. et al. Gas/vapour separation using ultra-microporous metal-organic frameworks: insights into the structure/separation relationship. *Chem. Soc. Rev.* **46**, 3402–3430 (2017).
15. Yang, L. et al. Energy-efficient separation alternatives: metal-organic frameworks and membranes for hydrocarbon separation. *Chem. Soc. Rev.* **49**, 5359–5406 (2020).
16. Wang, H. & Li, J. Microporous metal-organic frameworks for adsorptive separation of C5-C6 alkane isomers. *Acc. Chem. Res* **52**, 1968–1978 (2019).
17. Barnett, B. R. et al. Recent progress towards light hydrocarbon separations using metal-organic frameworks. *Trends Chem.* **1**, 159–171 (2019).
18. Zhao, X. et al. Metal-organic frameworks for separation. *Adv. Mater.* **30**, 1705189 (2018).
19. Zeng, H. et al. Orthogonal-array dynamic molecular sieving of propylene/propane mixtures. *Nature* **595**, 542–548 (2021).
20. Zhang, P. et al. Ultramicroporous material based parallel and extended paraffin nano-trap for benchmark olefin purification. *Nat. Commun.* **13**, 4928 (2022).
21. Jiang, Y. et al. Comprehensive pore tuning in an ultrastable fluorinated anion cross-linked cage-like MOF for simultaneous benchmark propyne recovery and propylene purification. *Angew. Chem. Int. Ed.* **61**, e202200947 (2022).
22. Peng, Y.-L. et al. Robust ultramicroporous metal-organic frameworks with benchmark affinity for acetylene. *Angew. Chem. Int. Ed.* **57**, 10971–10975 (2018).

23. Zhang, Y. et al. Rational design of microporous MOFs with anionic boron cluster functionality and cooperative dihydrogen binding sites for highly selective capture of acetylene. *Angew. Chem. Int. Ed.* **59**, 17664–17669 (2020).
24. Lin, R.-B. et al. Optimized separation of acetylene from carbon dioxide and ethylene in a microporous material. *J. Am. Chem. Soc.* **139**, 8022–8028 (2017).
25. Zhang, Z.-Q. et al. Hexafluorogermanate (GeFSIX) anion-functionalized hybrid ultramicroporous materials for efficiently trapping acetylene from ethylene. *Ind. Eng. Chem. Res.* **57**, 7266–7274 (2018).
26. Ke, T. et al. Molecular sieving of C_2-C_3 alkene from alkyne with tuned threshold pressure in robust layered metal-organic frameworks. *Angew. Chem. Int. Ed.* **59**, 12725–12730 (2020).
27. Yang, L. et al. Adsorption site selective occupation strategy within a metal-organic framework for highly efficient sieving acetylene from carbon dioxide. *Angew. Chem. Int. Ed.* **60**, 4570–4574 (2021).
28. Niu, Z. et al. A MOF-based ultra-strong acetylene nano-trap for highly efficient C_2H_2/CO_2 separation. *Angew. Chem. Int. Ed.* **60**, 5283–5288 (2021).
29. Zhang, L. et al. Benchmark C_2H_2/CO_2 Separation in an Ultra-Microporous Metal-Organic Framework via Copper(I)-Alkynyl Chemistry. *Angew. Chem. Int. Ed.* **60**, 15995–16002 (2021).
30. Wang, L. et al. Interpenetration symmetry control within ultra-microporous robust boron cluster hybrid MOFs for benchmark purification of acetylene from carbon dioxide. *Angew. Chem. Int. Ed.* **60**, 22865–22870 (2021).
31. Di, Z. et al. Cage-like porous materials with simultaneous High C_2H_2 storage and excellent C_2H_2/CO_2 separation performance. *Angew. Chem. Int. Ed.* **60**, 10828–10832 (2021).
32. Lou, W. et al. Screening Hoffman-type metal organic frameworks for efficient C_2H_2/ CO_2 separation. *Chem. Eng. J.* **452**, 139296 (2023).
33. Xu, Z. et al. A robust Th-azole framework for highly efficient purification of C_2H_4 from a $C_2H_4/C_2H_2/C_2H_6$ mixture. *Nat. Commun.* **11**, 3163 (2020).
34. Gu, X.-W. et al. Immobilization of lewis basic sites into a stable ethane-selective mof enabling one-step separation of ethylene from a ternary mixture. *J. Am. Chem. Soc.* **144**, 2614–2623 (2022).
35. Cao, J.-W. et al. One-step ethylene production from a four-component gas mixture by a single physisorbent. *Nat. Commun.* **12**, 6507 (2021).
36. Mukherjee, S. et al. Amino-functionalised hybrid ultra-microporous materials that enable single-step ethylene purification from a ternary mixture. *Angew. Chem. Int. Ed.* **60**, 10902–10909 (2021).
37. Dong, Q. et al. Tuning gate-opening of a flexible metal-organic framework for ternary gas sieving separation. *Angew. Chem. Int. Ed.* **59**, 22756–22762 (2020).
38. Dong, Q. et al. Shape- and size-dependent kinetic ethylene sieving from a ternary mixture by a trap-and-flow channel crystal. *Adv. Funct. Mater.* **32**, 2203745 (2022).
39. Xiong, X.-H. et al. Nitro-decorated microporous covalent organic framework (TpPa-NO_2) for selective separation of C_2H_4 from a C_2H_2/ C_2H_4/CO_2 mixture and CO_2 capture. *ACS Appl. Mater. Interfaces* **14**, 32105–32111 (2022).
40. Li, H. et al. An unprecedented pillar-cage fluorinated hybrid porous framework with highly efficient acetylene storage and separation. *Angew. Chem. Int. Ed.* **60**, 7547–7552 (2021).
41. Cui, X. et al. Pore chemistry and size control in hybrid porous materials for acetylene capture from ethylene. *Science* **353**, 141–144 (2016).
42. Li, B. et al. An ideal molecular sieve for acetylene removal from ethylene with record selectivity and productivity. *Adv. Mater.* **29**, 1704210 (2017).
43. Xu, N. et al. A TIFSIX pillared MOF with unprecedented zsd topology for efficient separation of acetylene from quaternary mixtures. *Chem. Eng. J.* **450**, 138034 (2022).
44. Wang, J. et al. Optimizing pore space for flexible-robust metal-organic framework to boost trace acetylene removal. *J. Am. Chem. Soc.* **142**, 9744–9751 (2020).
45. Hutter, J. et al. $_{CP}2_K$: atomistic simulations of condensed matter systems. *WIREs Comput. Mol. Sci.* **4**, 15–25 (2014).
46. Perdew, J. P. et al. Generalized gradient approximation made simple. *Phys. Rev. Lett.* **77**, 3865–3868 (1996).
47. Hartwigsen, C. et al. Relativistic separable dual-space Gaussian pseudopotentials from H to Rn. *Phys. Rev. Lett.* **58**, 3641–3663 (1998).
48. VandeVondele, J. et al. Gaussian basis sets for accurate calculations on molecular systems in gas and condensed phases. *J. Chem. Phys.* **127**, 114105 (2007).
49. Klimeš, J. et al. Perspective: Advances and challenges in treating van der Waals dispersion forces in density functional theory. *J. Chem. Phys.* **137**, 120901 (2012).

Acknowledgements

This work was supported by the National Natural Science Foundation of China (Nos. 21908193 and 22205207) and Jinhua Industrial Key Project (2021A22648). We thank the help of Dr. Yunlei Peng from CUP.

Author contributions

Y.J. and Y.H. contributed equally to this work. Y.Z. designed and guided the project. Y.J. and Y.H. designed and synthesized the materials, performed the majority of the structural characterization, collected gas sorption data and conducted breakthrough experiments. B. L. conducted the DFT calculations. L.W. and H.N. collected X-ray diffraction data and solved the structures. R.K. performed the IAST and Q_{st} calculation. Y.J. and Y.Z. draft the paper. X.H. provided important advice and revised the paper. All authors contributed to the discussion of results and commented on the paper.

Competing interests

The authors declare no competing interests.

Additional information

Supplementary information The online version contains supplementary material available at https://doi.org/10.1038/s41467-023-35984-5.

Correspondence and requests for materials should be addressed to Yuanbin Zhang.

Peer review information *Nature Communications* thanks Zhang-Wen Wei, Soumya Mukherjee and the other, anonymous, reviewer(s) for their contribution to the peer review of this work. Peer reviewer reports are available.